ELSEVIER

Polymer 42 (2001) 2627–2636

polymer

www.elsevier.nl/locate/polymer

Evaluating the energetics of dilatational band growth under biaxial loading conditions

A.B. Sabbagh, A.J. Lesser*

Department of Polymer Science and Engineering, University of Massachusetts, Amherst, MA 01003, USA

Received 11 February 2000; received in revised form 1 May 2000; accepted 2 May 2000

Abstract

Post-yield, heterogeneous deformation in the form of dilatational bands (DB's) develops in blown, linear low density polyethylene films under certain biaxial loading conditions. The material within the dilatational bands is drawn transverse to the initial orientation direction. The films typically exhibit a two-stage drawing process associated with migration of the DB boundary into the undrawn material and subsequent deformation of the drawn material within the DB. Kinematic measurements reveal that DB's evolve primarily by isotropic expansion with distortion occurring to a smaller extent. Correspondingly, the *M* integral is used to determine the energy release rate associated with isotropic expansion of the DB under various biaxial stress states. A thermodynamic model incorporating the *M* integral is used to determine a material property that describes the energy associated with the drawing process. The *M* integral and the thermodynamic model appear to describe DB evolution well. © 2000 Published by Elsevier Science Ltd.

Keywords: Polyethylene; Biaxial; Deformation

1. Introduction

In a previous paper, we report the development of a heterogeneous post-yield deformation in the form of dilatational bands that occur in blown, linear low density polyethylene (LLDPE) films subjected to certain biaxial loading conditions [1]. Dilatational bands are regions of highly drawn material embedded within the original, untransformed material, much like a neck in a tensile specimen. As depicted in Fig. 1, the drawing direction within the dilatational band is transverse to the initial, far-field orientation direction. The drawn and undrawn regions are separated by a sharp boundary with the properties being distinctly different between the regions. Hence, the deformation is heterogeneous, and for modeling purposes the dilatational band may be macroscopically treated as a separate phase within the original material. Although the phenomenology between heterogeneous biaxial deformation and uniaxial necking are similar, the kinematics of each of process are not. Necking involves a single stage drawing process where boundary migration is due primarily to the consumption of undrawn material at the neck boundary. Dilatational band evolution involves two drawing processes occurring simultaneously; consumption of undrawn material and the continued deformation of the drawn material within the dilatational band.

Dilatational bands mechanically resemble cracks which carry tractions across their surface, much like crazes. Furthermore, almost all of the transformation occurs within the boundary of the dilatational band. Based on these observations, one can make use of certain fracture mechanics principles to model this drawing process. The *J* contour integral has been used extensively to describe crack propagation in materials [2–5]. Other contour integrals have also been defined by Knowles and Sternberg to describe other elementary motions associated with the evolution of crack and/or process zones [6–8]. These are the *L* and *M* integrals, which are defined as the energy release rates associated with rotation and expansion, respectively. Chudnovsky has also introduced the *N* integral as the energy release rate associated with distortion [9]. These contour integrals have been incorporated into a thermodynamic model developed by Chudnovsky [10]. The thermodynamic model relates the energy due to entropy production to the energy consumed in crack and process zone evolution via the elementary motions of translation, expansion, distortion and rotation. The material property in this model is the specific enthalpy of transformation, γ, which is the energy per unit volume required to transform a material from an initial state to a final state. Thus, the specific enthalpy of transformation is a measure of the material's ability to resist transformation.

* Corresponding author. Tel.: +1-413-577-0433; fax: +1-413-545-0082.
E-mail address: ajl@polysci.umass.edu (A.J. Lesser).

0032-3861/01/$ - see front matter © 2000 Published by Elsevier Science Ltd.
PII: S0032-3861(00)00367-0

Nomenclature

C_1	fitting parameter for stress relaxation
C_2	fitting parameter for stress relaxation
$\dot{D}$	rate of dissipation
F	strain energy
$\dot{F}$	rate of strain energy
J_k	J integral
L	L integral
M	M integral
N_{kl}	N integral
P	system pressure
$\dot{P}$	rate of measured pressure change
P_{SR}	pressure in system if only stress relaxation were present
$\dot{P}_{SR}$	rate of pressure change due to stress relaxation
R_0	amount of transformation associated with expansion
$\dot{S}_i$	rate of internal entropy production
T	temperature
V^*	system volume while at constant volume
X^{TR}	thermodynamic force associated with translation
X^{EXP}	thermodynamic force associated with expansion
X^{DIS}	thermodynamic force associated with distortion
$\dot{a}$	rate of translation
b	film thickness
d_{kl}	distortion
$\dot{d}_{kl}$	rate of distortion
e	isotropic expansion
$\dot{e}$	rate of isotropic expansion
ℓ	1/2 the dilatational band length
ℓ_0	1/2 the initial dilatational band length
w	1/2 the dilatational band width
w_i	irreversible work
$\dot{w}_i$	rate of irreversible work
w_0	1/2 the initial dilatational band width
α_1	fitting parameter for stress relaxation
α_2	fitting parameter for stress relaxation
β	fraction of $(PV)^*$ recovered
γ	specific enthalpy of transformation
γ^{oct}	octahedral shear strain
λ_i	draw ratio

Chudnovsky has successfully applied this model to a variety of polymer systems subjected to various loading conditions [11–14].

The objective of this paper is to compare the energetics of heterogeneous, post-yield deformation of several polyethylene films under various biaxial loading conditions. We use a thermodynamic approach to model the phenomenon of heterogeneous deformation and to determine γ. We also compare the effects of stress state, film composition, microstructure and orientation on the energetics of heterogeneous deformation.

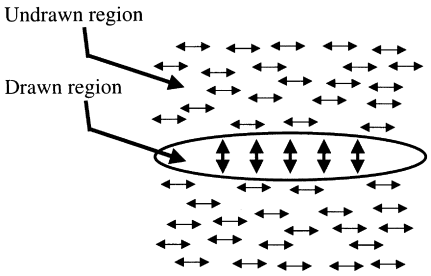

Fig. 1. Schematic showing orientation of drawn material within original, undrawn material.

2. Experimental

2.1. Materials

Four polyethylene films were used in this research. Exxon supplied two linear low-density polyethylene (LLDPE) blown films. One Exxon polyethylene resin was prepared

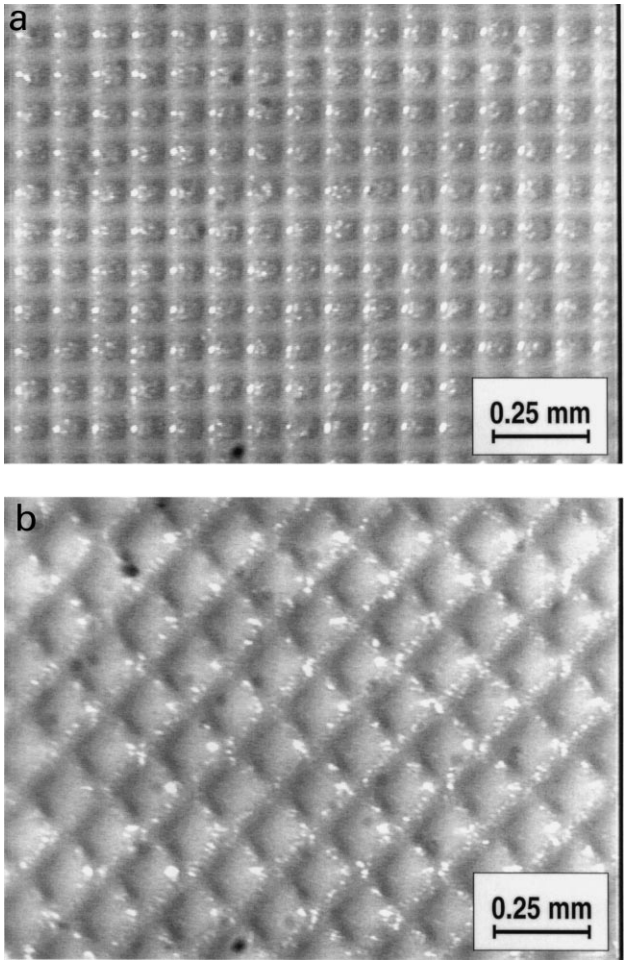

Fig. 2. Embossing patterns on Procter and Gamble films: (a) square patterns on film C; (b) diamonds patterns on film D.

Table 1
Property data for films A–D

	Film A	Film B	Film C	Film D
Percent Crystallinity	28.8	31.7	22.7	28.4
Melting point (°C)	126.1	116.0	123.5	114.3
Thickness (μm)	75	75	27	27
Orientation, *f*	0.00297	0.000866	0.013	0.202
Orientation direction	MD	MD	MD	MD
Filler	N/A	N/A	TiO_2 (1–4 wt.%)	TiO_2 (1–4 wt.%)
Embossing pattern	N/A	N/A	Squares	Diamonds
Catalyst	Ziegler–Natta	Metallocene	Unknown	Unknown
Opacity	Clear	Clear	White	White

using a conventional Ziegler–Natta catalyst (film A) while the other resin was made using a metallocene based catalyst (film B). The metallocene based resin has well controlled branching, while the Ziegler–Natta based resin has branches which are much more randomly placed along the main chain. The blowing process imparts a slight orientation along the machine direction (MD) in the films. Both Exxon films are nominally 75 μm thick.

Proctor and Gamble (P&G) provided two, TiO_2 filled (1–4 wt.%) polyethylene films. These films have patterns embossed on them, with film C having a square pattern and film D having a diamond pattern (see Figs. 2a and b, respectively). Film C is solution cast and subsequently drawn while film D is blown. Both films are oriented along the MD, with film D having a much higher orientation than the other films. The P&G films are nominally 27 μm thick.

Property data for the films are given in Table 1. An Olympus BX60 polarizing microscope equipped with a U-CTB thick Berek type calcite tilt compensator was used to determine the birefringence of the Exxon films. Wide angle X-ray scattering (WAXS) was used to determine the orientation direction. The WAXS instrument employs a graphite monochromated Cu–Kα radiation source with a Siemens GADDS multi-line gas-filled area detector. A helium chamber was also used to reduce air scatter. All WAXS measurements were through the thickness of the film. The orientation functions for the Exxon films were determined assuming a theoretical birefringence for polyethylene of 0.059[15,16]. Infrared (IR) dichroism was used to determine the initial orientation in the P&G films using a Perkin Elmer Spectrum 2000 FT-IR spectrometer. The 720 cm^{-1} peaks of the IR spectra were used to determine the dichroic ratio, from which the orientation functions were calculated [17]. The melting point and percent crystallinity were measured using differential scanning calorimetry (DSC) at a heating rate of 10°C/min for all films.

2.2. Biaxial testing

A schematic of the biaxial testing equipment is shown in Fig. 3. The film is placed between a polycarbonate base and a stainless steel template containing a circular or elliptical hole and an O-ring seal. Water is pumped through a small hole in the polycarbonate base using a Cole Parmer 7553-70 peristaltic pump, forcing the film to deform in a blister type fashion. The hydrostatic pressure exerted by the water places the portion of film away from the boundary in a biaxial state of stress. An equibiaxial stress state is created

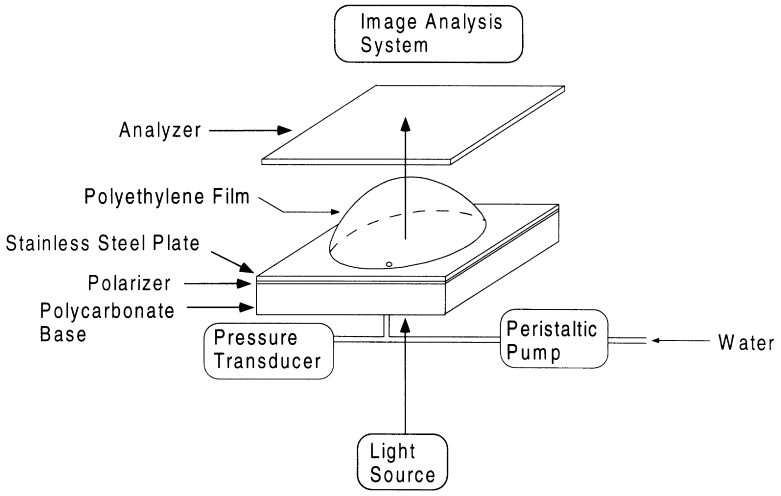

Fig. 3. Schematic of the biaxial testing equipment.

by using a template with a circular hole (15.2 cm diameter), so that the principle stresses are of the same magnitude (i.e. $\sigma_1 = \sigma_2$). Other biaxial loading conditions are created by using templates having elliptically shaped holes with the major to minor axes ($2a \times 2b$) given by $15.2 \times 7.6\ \text{cm}^2$ and $15.2 \times 5.1\ \text{cm}^2$, producing principle stresses of $\sigma_1 = 2\sigma_2$ and $\sigma_1 = 3\sigma_2$, respectively. All tests are conducted at room temperature and at a strain rate of $0.05\ \text{min}^{-1}$. Each film specimen is loaded until a dilatational band has formed to a suitable size (e.g. 25–50 mm in length) and then is allowed to evolve at constant volume for 30 s. During this time the pressure in the blister is measured and digital images of the dilatational bands are acquired at a rate of 2 images per second. The films are then unloaded.

Initial experiments showed that several dilatational bands may typically initiate and coalesce in these films during biaxial loading, which presents difficulties when modeling the process. Therefore, a defect is placed in each film prior to testing so that only one dilatational band initiates. The defect is created by locally heating the film with a 12.7 mm diameter aluminum rod at 100°C. The rod is placed at the center of the sample such that it's length is coincident with the orientation direction of the film. A 60 μm thick polyimide film is placed between the rod and polyethylene sample.

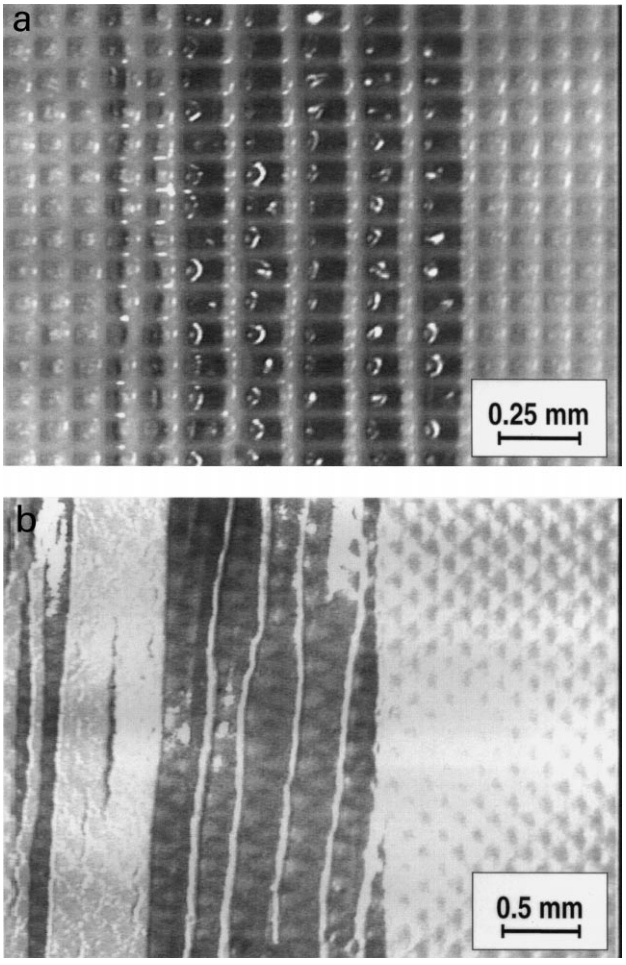

Fig. 4. Close-up images of dilatational bands show material drawn along the transverse direction: (a) film C; (b) film D.

Table 2
Nomenclature for films subjected to various biaxial stress states

	$\sigma_1 \perp$ MD $\sigma_1 = 2\sigma_2 \sigma_1 = \sigma_2$		$\sigma_1 \parallel$ MD $\sigma_1 = 2\sigma_2$
Film A	Film A-SS 2:1 ⊥	Film A-SS 1:1	Film A-SS 2:1 ∥
Film B	Film B-SS 2:1 ⊥	Film B-SS 1:1	Film A-SS 2:1 ∥
Film C	Film C-SS 2:1 ⊥	Film C-SS 1:1	Film A-SS 2:1 ∥
Film D	Film D-SS 2:1 ⊥	Film D-SS 1:1	Film A-SS 2:1 ∥

3. Discussion of results

We study the effect of three stress states on the dilatational band evolution in these films. The nonequibiaxial stress state having a 2:1 ratio in the magnitude of the principle stresses with the higher principle stress being aligned transverse to the initial orientation direction is referred to as SS 2:1 ⊥. The equibiaxial stress state is referred to as SS 1:1. The nonequibiaxial stress state having a 2:1 ratio in the principle stresses with the higher principle stress being aligned with the initial orientation direction is referred to as SS 2:1 ∥. The nomenclature for the films and stress states is summarized in Table 2.

3.1. Kinematics

A kinematic analysis of the deformation may be obtained through measurements of the dilatational band dimensions and the principle draw ratios. Global kinematics give the rate of boundary migration and were determined from the length (2ℓ) and width ($2w$) of the dilatational band as a function of time. Local kinematics, as determined from principle draw ratios within the dilatational band, provide information as to how local deformation relates to the overall changes in dilatational band dimensions.

Local kinematics for films C and D were determined from the principle draw ratios. Close-up images of the dilatational bands in films C and D are shown in Figs. 4a and b, respectively. From these images one can see the drawn square and diamond grid patterns within the dilatational band. The draw ratios in the $2w$ direction (λ_2) and 2ℓ direction (λ_1) were measured from the change in dimensions of these embossed patterns. The thickness draw ratio (λ_3) was then calculated assuming the drawing is a constant volume process (i.e. $\lambda_1\lambda_2\lambda_3 = 1$). This assumption is based on results obtained earlier with the Exxon LLDPE films, and is probably reasonable for these films considering the low filler content [1]. Note in Fig. 4b that the dilatational band boundary is quite sharp and not affected by the preplaced diagonal pattern, which indicates that the orientation imparted earlier in the processing of the films has a much greater effect on the deformation behavior than the solid state embossing which occurred later in the processing.

Fig. 5 shows a plot of the principle draw ratios for film C

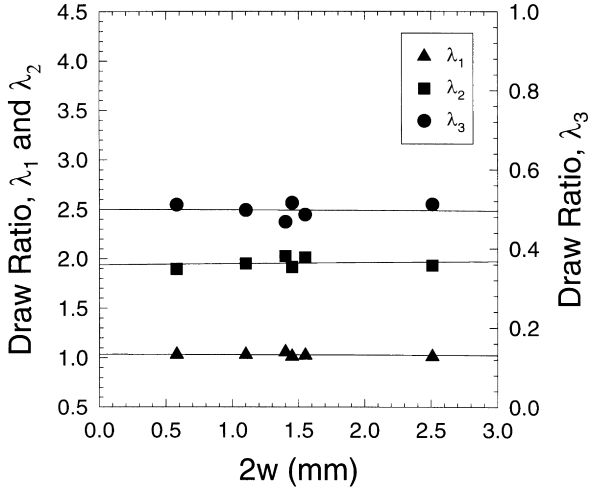

Fig. 5. Principle draw ratios measured in dilatational bands as a function of 2*w* for film C under SS 2:1 ⊥.

as a function of 2*w* at constant volume for SS 2:1 ⊥. The draw ratios remain essentially constant with time, which is also typical of neck propagation in uniaxial drawing. Identical results are observed for film C under SS 1:1 and SS 2:1 ∥ as well. However, the principle draw ratios measured in film D indicate the presence of an additional drawing process. Figs. 6a–c show plots of the draw ratios for film D under SS 2:1 ⊥–SS 2:1 ∥, respectively. The plots indicate that the draw ratios here evolve via a two-stage drawing process. A set of draw ratios is established upon the initiation of a dilatational band. The draw ratios then continue to evolve as the dilatational band increases in size. The width draw ratio (λ_2) increases while the thickness draw ratio (λ_3) decreases. That is, the material within the band is becoming more oriented along the 2*w* direction while the thickness of the band is decreasing. The draw ratio along the 2ℓ direction (λ_1) does not change significantly during the evolution. The two-stage drawing process with film D was also observed in the Exxon films (films A and B) under SS 1:1 [1]. Finally, note that the rate of the second drawing stage is greatest for SS 2:1 ⊥, followed by SS 1:1, and then by SS 2:1 ∥. This is expected, since SS 2:1 ⊥ is the loading condition which is most favorable to heterogeneous drawing, while SS 2:1 ∥ is least favorable.

The octahedral shear strain is a convenient way to collapse the draw ratio data into a measure of the overall amount of shape change within the material. The draw ratios are used to calculate the principle strains within the drawn material and the principle strains, in turn, are used to calculate the octahedral shear strain (γ_{oct}). Fig. 7 shows γ_{oct} plotted as a function of 2*w* for films C and D. As with the draw ratio plots, film C does not show an increase in shear deformation with increasing 2*w*. However, the increase in γ_{oct} with 2*w* in film D indicates the presence of the two-stage drawing process. Furthermore, this effect is found to be greatest for SS 2:1 ⊥, followed by SS 1:1, and then by SS 2:1 ∥, as determined by the rate of increase in γ_{oct} with 2*w*.

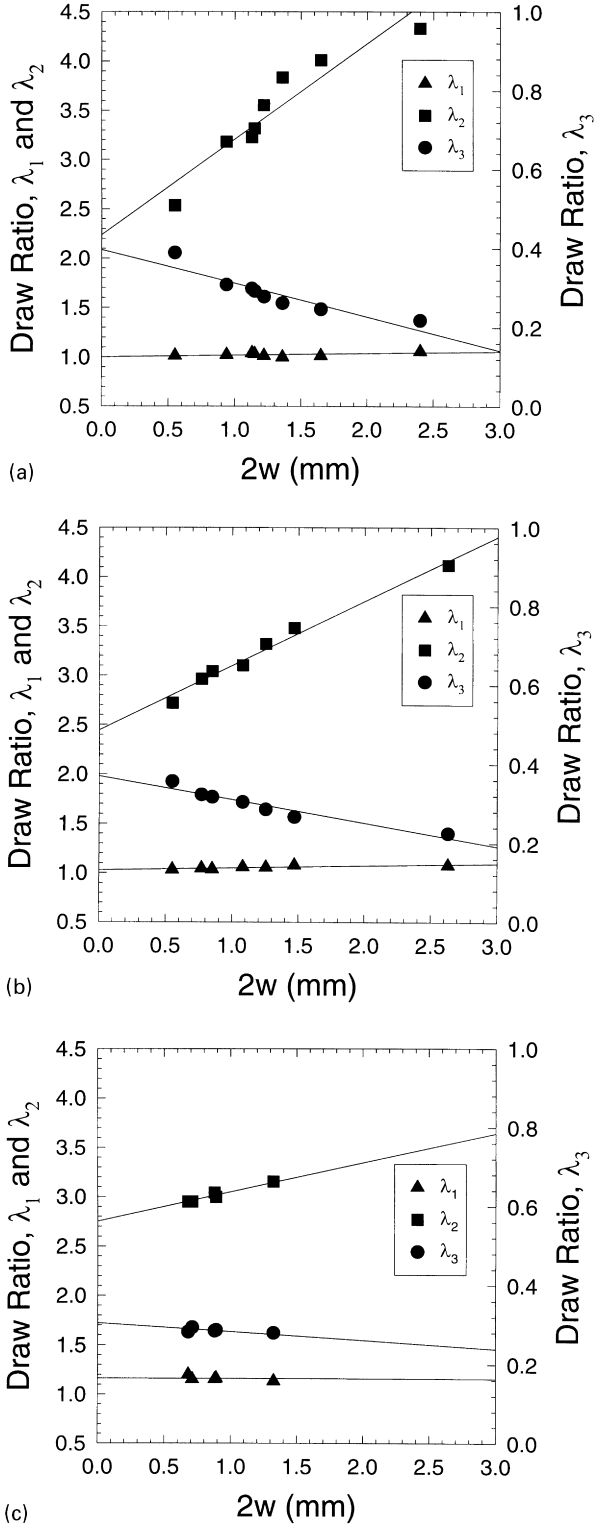

Fig. 6. Principle draw ratios measured in dilatational bands as a function of 2*w* for film D: (a) SS 2:1 ⊥; (b) SS 1:1; (c) SS 2:1 ∥.

Fig. 7 also shows that film D undergoes a much greater amount of total shape change than film C, which is not immediately obvious in the draw ratio plots. Although not done here, the octahedral shear strain may be incorporated

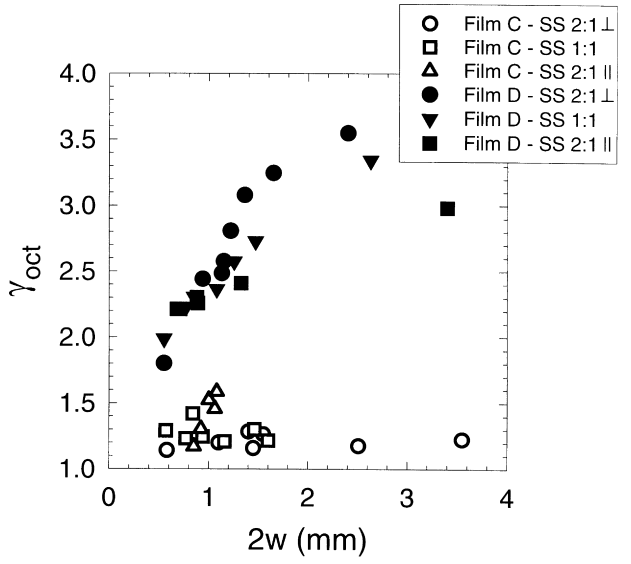

Fig. 7. Octahedral shear strain measured in dilatational bands as a function of 2*w* for films C and D under SS 2:1 ⊥–SS 2:1 ||.

into a transformation parameter, which would, in turn, quantify the extent of transformation upon drawing for each film. This would be necessary for making comparisons of the specific enthalpy of transformation for materials having different initial and final states.

Dilatational bands dimensions (i.e. 2ℓ and $2w$) were measured as a function of time under constant volume for films C and D to determine the global kinematics. Note from Eq. (1) that the deformation tensor may be decomposed into symmetric (expansion) and antisymmetric (distortion) components. These expressions for expansion and distortion were used to determine from the data the dominant elementary motion associated with dilatational band growth. This, in turn, is used to determine how the thermodynamic model will be applied.

$$\underset{\text{Total Distortion}}{\begin{bmatrix} \frac{\ell}{\ell_0} & 0 \\ 0 & \frac{w}{w_0} \end{bmatrix}} = \underset{\text{Expansion}}{\tfrac{1}{2}\left[\frac{\ell}{\ell_0} + \frac{w}{w_0}\right]\begin{bmatrix} 1 & 0 \\ 0 & 1 \end{bmatrix}} + \underset{\text{Distortion}}{\tfrac{1}{2}\left[\frac{\ell}{\ell_0} - \frac{w}{w_0}\right]\begin{bmatrix} 1 & 0 \\ 0 & -1 \end{bmatrix}} \quad (1)$$

Figs. 8a–c show plots of the scalar components of the expansion rate and distortion rate tensors of the dilatational bands for film D as a function of time at constant volume under SS 2:1 ⊥–SS 2:1 ||, respectively. The expansion rates are noticeably higher than the distortion rates. Similar results are also observed for films A–C. Based on these observations, we make a first order approximation by only considering the expansion term in the thermodynamic model, which is discussed in more detail in the next section.

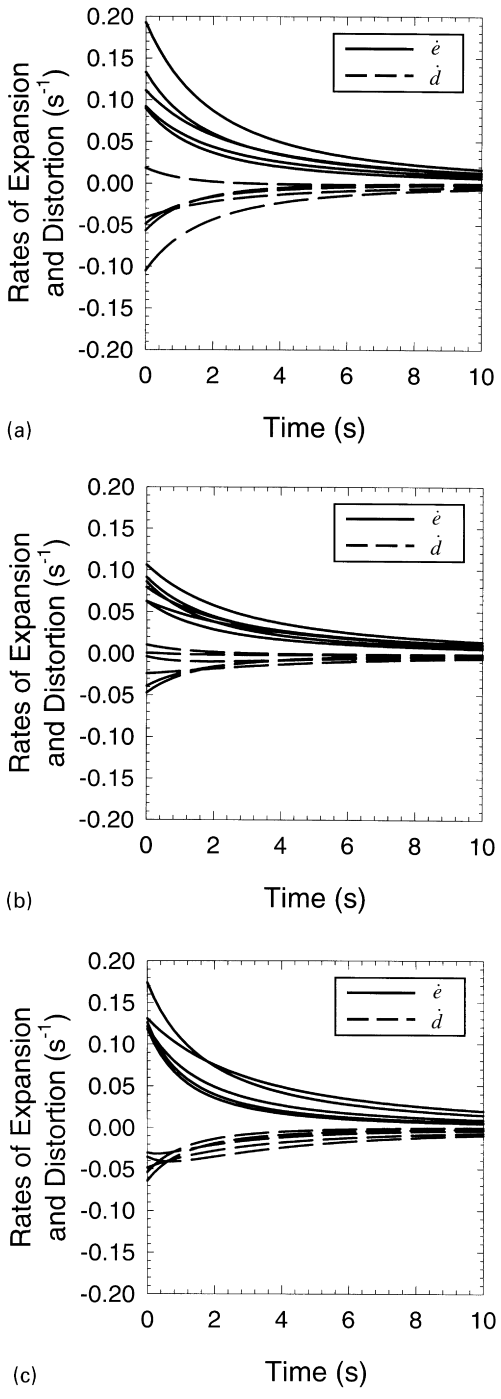

Fig. 8. Expansion and distortion rates for several dilatational bands in film D: (a) SS 2:1 ⊥; (b) SS 1:1; (c) SS 2:1 ||.

3.2. Energetics

The evolution of heterogeneous deformation in these films is modeled within a thermodynamic framework. The thermodynamic model incorporates elements of thermodynamics and fracture mechanics to yield the rate expression shown in Eq. (2). The energy associated with entropy production is related to the energy consumed by crack

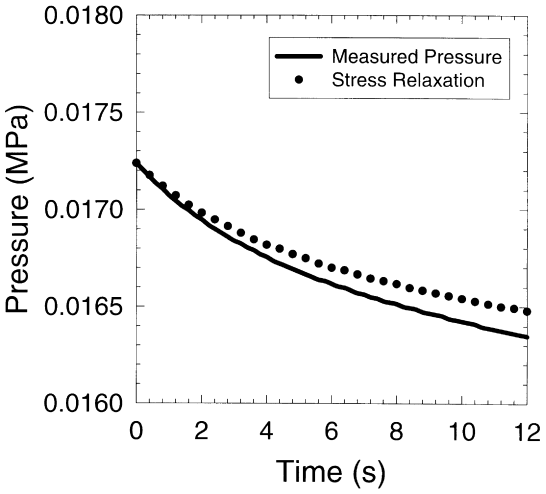

Fig. 9. Pressure measured in the blister as a function of time at constant volume for film B-SS 1:1. The extrapolated stress relaxation response is also plotted.

and/or process zone evolution via translation, expansion, distortion, etc. [6].

$$T\dot{S}_i = \dot{a}X^{TR} + \dot{e}X^{EXP} + \dot{d}_{kl}X^{DIS} + \dot{D} \tag{2}$$

The global kinematics show that isotropic expansion is the primary elementary motion associated with dilatational band growth. Reducing Eq. (2) to a one parameter model with only expansion, and then expanding X^{EXP} into active and resistive components, Eq. (2) reduces to:

$$T\dot{S}_i = \dot{e}(M - \gamma R_0) + \dot{D} \tag{3}$$

where $\dot{e}$ is the isotropic expansion rate, M is the energy release rate associated with isotropic expansion (M integral), R_0 is the resistive moment (i.e. the dilatational band area in this case), and $\dot{D}$ represents any other dissipative processes. Note that this model was originally developed to model fracture processes. In these cases, the thermodynamic model reduces to a one parameter equation involving the J integral. Here we have adapted the model to describe a yielding process, which consequently provides a unique opportunity to use the M integral. For constant volume conditions, the M integral is defined by Eq. (4),

$$M|_V = \frac{-1}{b}\frac{\partial F}{\partial ; e} \tag{4}$$

where F is the strain energy.

The energetics of constant volume dilatational band growth were studied in this research. Film samples were loaded until a dilatational band formed. The loading was then stopped so that the system was at constant volume. While at constant volume, the strain energy in the system provided the driving force that allowed the dilatational band to continue to evolve. Fig. 9 shows the pressure drop occurring with time for a film B-SS 1:1 sample associated with a loss in strain energy. Note that the strain energy in the film diminishes with time due to two processes occurring simultaneously; dilatational band growth and far-field stress relaxation. Therefore a viscoelastic component is added to the model to account for stress relaxation. The following equation is derived from Eq. (3) (see Appendix A) and gives a linear expression in terms of experimentally measurable variables:

$$\dot{e} = \frac{\beta V^*}{b\gamma R_0}[\dot{P}_{SR} - \dot{P}] \tag{5}$$

where $\dot{P}$ is the rate of change in the measured pressure, $\dot{P}_{SR}$ is the rate of change in pressure due to far-field stress relaxation, b is the film thickness, β is the fraction of $(PV)^*$ that is recoverable upon unloading and $(PV)^*$ is the PV just before unloading. The inverse of the slope yields γ.

The rate of pressure drop due to stress relaxation in Eq. (5) is extrapolated from independent stress relaxation experiments. In these experiments, films were loaded to various pressure levels below that required for dilatational band growth, and then allowed to relax at constant volume. The relaxation was modeled with a two term exponential decay, as shown below:

$$P = C_1\, e^{(-\alpha_1 t)} + C_2\, e^{(-\alpha_2 t)} \tag{6}$$

The effect of pressure on the parameters C_1, C_2, α_1 and α_2 is determined and extrapolated to the pressure at which the dilatational band forms. The extrapolated stress relaxation response for the film B sample in Fig. 9 is also plotted. This plot shows that most of the pressure change occurs due to far-field stress relaxation. Note however that volume of the dilatational band is only between 1 and 35 of the total volume of film. Normalizing the strain energy spent during stress relaxation and dilatational band growth by the respective mass of material involved gives a significantly higher energy per unit mass for drawing, which is expected considering the greater amount of deformation that occurs during drawing.

A series of digital images obtained of a dilatational band during constant volume growth is shown in Fig. 10 for the film B-SS 1:1 sample. The images are analyzed using Zeiss Image Analysis software. The length (2ℓ) and width ($2w$) are measured as a function of time and normalized by the initial $2\ell_0$ and $2w_0$. Plots of ℓ/ℓ_0 and w/w_0 are shown in Fig. 11. Note that the rates of change in ℓ/ℓ_0 and w/w_0 decrease with time as strain energy diminishes due to dilatational band growth and stress relaxation. This is also seen in the rate of isotropic expansion, which is also plotted in Fig. 11.

The M integral is now determined as the change in strain energy with respect to isotropic expansion. The M integral is plotted in Fig. 12 for the film B-SS 1:1 sample. The strain energy decreases with time but the expansion decreases at a faster rate such than M increases. The dilatational band eventually stops growing, as shown by Fig. 11, indicating that dilatational band growth is a stable process under constant volume conditions.

The resistive component, R_0, reduces to the dilatational

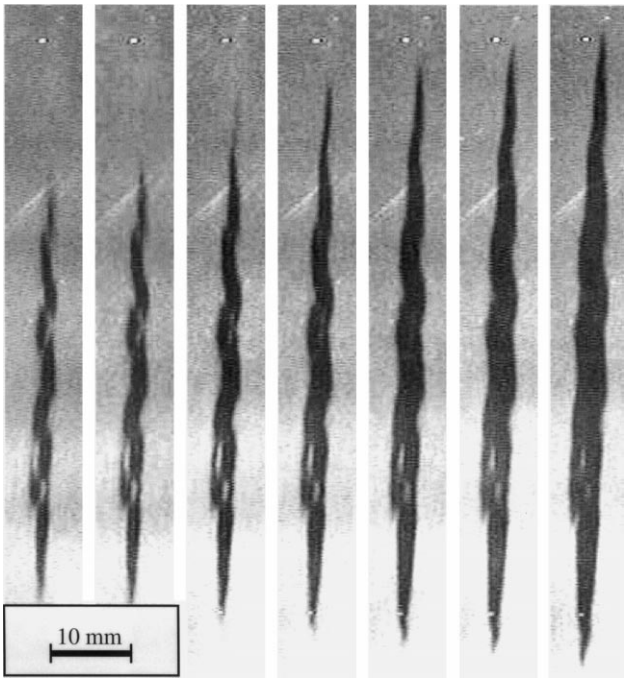

Fig. 10. Series of images showing dilatational band evolution at constant volume for film B-SS 1:1.

band area, which is shown in Fig. 13 to increase much like ℓ/ℓ_0 and w/w_0 as a function of time. Following the dilatational band evolution, the films are unloaded so that the strain energy remaining in the system may be measured. Eq. (5) is now used to determine γ. The appropriate data are plotted for the film B-SS 1:1 sample in Fig. 14 to yield the linearized trend predicted by Eq. (5). From the slope, γ is determined for this sample to be 6.01 MJ/m^3.

Table 3 gives the calculated values of γ for all films and stress states. The values for γ range from 2 to 9 MJ/m^3. Note that several tests were also conducted in an attempt to create a single dilatational band without the presence of a prescribed defect. In these cases, the values obtained for γ were found to not differ from the those obtained with samples containing a defect. This lends confidence to the initial assumption that the defect does not influence the drawing behavior and ultimately the values obtained for γ. Physically, γ represents the energy required to transform a unit volume of material from some initial state to some final state. Before making any comparative statements, one must recognize that different initial and final orientations within each case will also contribute to the differences in γ. However, a few key observations are still made from Table 3. With the exception of the metallocene film, the equibiaxial stress state requires the least amount of energy necessary to draw dilatational bands. Therefore, to minimize the initiation and evolution of heterogeneous deformation, nonequibiaxial stress states are preferred over equibiaxial stress states. Note that the reverse trend is observed with the metallocene film. More tests are planned to determine how various materials and loading conditions result in differences in the energetics associated with drawing. Finally, note that heterogeneous deformation does not occur with the slightly oriented Exxon films under certain nonequibiaxial stress state. In the more highly oriented P&G films, one may be able to suppress heterogeneous deformation by applying even higher ratios of the principle stresses (e.g. 7:1).

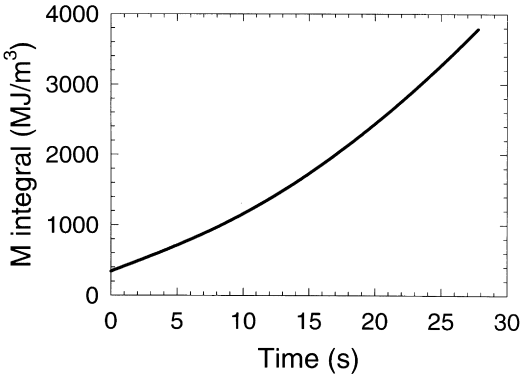

Fig. 12. The *M* integral for film B-SS 1:1 plotted as a function of time at constant volume.

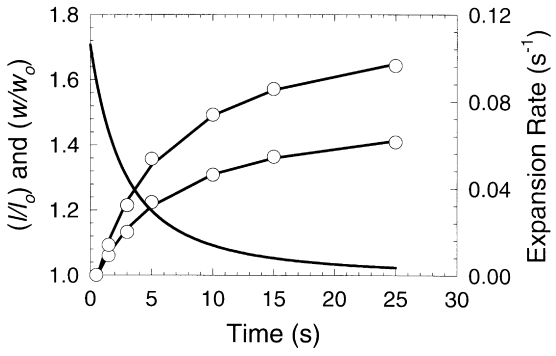

Fig. 11. Relative increase in dilatational band dimensions for film B-SS 1:1 as measured by ℓ/ℓ_0 and w/w_0. The expansion rate is determined from these and also plotted.

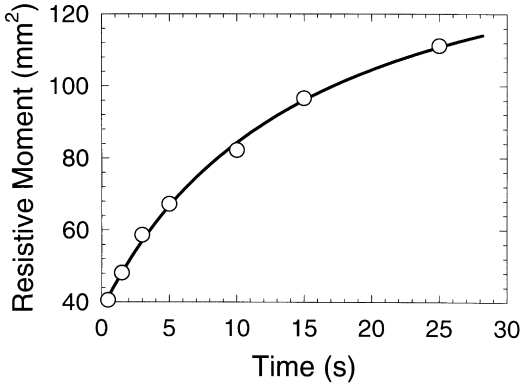

Fig. 13. The resistive moment (dilatational band area) as a function of time for film B-SS 1:1.

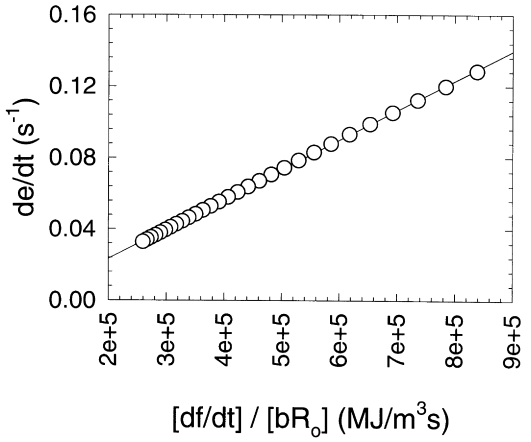

Fig. 14. Experimental data for film B-SS 1:1 is plotted in linearized form to obtain γ.

4. Conclusions

Dilatational band evolution in films A–D occurs primarily by isotropic expansion and to a smaller extent by distortion. Dilatational band boundary migration in film D for all stress states occurs by both consumption of undrawn material at the dilatational band boundary together with the continued deformation of the drawn material within the dilatational band. This is consistent with earlier results on film A-SS 1:1 and film B-SS 1:1. However, film C exhibits a one stage drawing process involving only consumption of new material at the boundary. Also, significantly higher shear deformation is observed for film D than with film C.

Values for the specific enthalpy of transformation, γ, range from 2 to 9 MJ/m^2. The one parameter thermodynamic model containing the M integral appears to describe the data well. The values for γ may be used to determine conditions, which are likely to either promote or inhibit heterogeneous deformation in polyolefin films.

Acknowledgements

The authors gratefully acknowledge Procter & Gamble for their financial support, Dr Todd Mansfield and Dr Emmett Crawford for their helpful suggestions and discussions, and Dr A.A. Stolov for his expertise in FT-IR characterization.

Appendix A

The strain energy while the system is at constant volume may be represented by

$$F(t) = \frac{\beta}{b} V^* P(t) \tag{A1}$$

where V^* is the volume of the system. The irreversible work that is dissipated as stress relaxation in the far-field

Table 3
The specific enthalpy of transformation, γ, determined for various films and stress states

	Specific enthalpy of transformation, γ (MJ/m^3)		
	SS 2:1 $\perp$	SS 1:1	SS 2:1 $\parallel$
Film A	5.29 ± 0.56	3.07 ± 0.72	n/a
Film B	3.82 ± 1.27	6.37 ± 1.10	n/a
Film C	4.82 ± 0.60	2.24 ± 0.72	8.56 ± 2.02
Film D	5.21 ± 0.80	2.60 ± 0.46	4.92 ± 1.15

is given by

$$w_i(t) = \frac{\beta}{b}(PV)^* - \frac{\beta}{b} P_{SR}(t) V^* \tag{A2}$$

From Eqs. (A1) and (A2), the rates of strain energy and irreversible work are

$$\dot{F}(t) = \frac{\beta}{b} V^* \dot{P}(t) \tag{A3}$$

$$\dot{w}_i(t) = \frac{-\beta}{b} V^* \dot{P}_{SR}(t) \tag{A4}$$

From the thermodynamic model with only expansion and applying the minimum entropy production principle [18,19]:

$$\dot{e}(\gamma R_0 - M) = 0 \tag{A5}$$

The M integral at constant volume in the presence of irreversible work is

$$M|_V = \frac{-\partial F}{\partial e} - \frac{\partial w_i}{\partial e} \tag{A6}$$

From Eqs. (A3)–(A4), we arrive at:

$$\dot{e} = \frac{\beta V^*}{b \gamma R_0} [\dot{P}_{SR} - \dot{P}] \tag{7}$$

References

[1] Sabbagh A, Lesser A. J Polym Sci, Part B: Polym Phys 1999;37:2651–63.
[2] Tjong SC. Polym Test 1997;16:563–74.
[3] Klemann BM, DeVilbiss T, Koutsky JA. Polym Engng Sci 1996;36:135–45.
[4] Lee C-B, Lu M-L, Chang F-C. J Appl Polym Sci 1993;47:1867–80.
[5] Tielking JT. Polym Test 1993;12:207–20.
[6] Knowles JK, Sternberg E. Arch Rational Mech Anal 1972;44:187–211.
[7] Freund LB. Int J Solids Struct 1978;14:241–50.
[8] Budiansky B, Rice JR. J Appl Mech 1973;40:201.
[9] Khandogin V, Chudnovsky A, Thermodynamics of Quasistatic Growth. In: Dynamics and Strength of Aircraft Constructions, Novosibirsk, vol 4, 1978. p. 148–75 (in Russian).
[10] Chudnovsky A, NASA Contractor Report 174634 Crack Layer Theory, March 1984.
[11] Aglan H, Chudnovsky A, et al. Int J Fract 1990;44:167–78.
[12] Kasakevich ML, Moet A, Chudnovsky A. Polymer 1990;31:435–9.

[13] Stojimirovic A, Kadota K, Chudnovsky A. J Appl Polym Sci 1992;46:1051–6.
[14] Chudnovsky A, Moet A. J Mater Sci 1985;20:630–5.
[15] Mead WT, Desper CR, Porter RS. J Polym Sci, Part B: Polym Phys 1979;17:859–92.
[16] Stein RS. J Polym Sci 1958;31:327.
[17] Read BE, Stein RS. Macromolecules 1968;31:16–126.
[18] Glansdorff P, Prigogine I. Thermodynamic theory of structure, stability, and fluctuations. New York: Wiley-Interscience, 1971.
[19] Jaynes ET. Ann Rev Phys Chem 1980;31:579–601.